Indian Journal of Engineering & Materials Sciences
Vol. 27, April 2020, pp. 431-437

A Unique pipe-like C_3N_4 with enhanced photocatalytic degradation of organic pollutant

Maxwell Selase Akple
Mechanical Engineering Department, Ho Technical University, P.O. Box HP 217, Ho, Volta Region, Ghana

Received: 04 December 2019; Accepted: 16 March 2020

Morphology tuning is one of the innovative techniques to overcome challenges of a pristine graphitic carbon nitride (g-C_3N_4) as a photocatalyst. In this study, a unique pipe-like C_3N_4 have been fabricated using a facile, environmentally friendly and scalable approach by treating dicyandiamide (DCDA) with ethylene glycol and nitric acid. The pipe-like C_3N_4 samples have been possessed unique structural morphology with enhanced visible light-harvesting ability, efficient charge separation and large surface area with more reactive sites. These enhanced properties of the pipe-like C_3N_4 have been exhibited superior complete photocatalytic degradation of methylene Blue (MB) within 30 min under visible light ($\lambda > 420$ nm) compared to the bulk C3N4. In addition, the pipe-like C_3N_4 have good photostability and efficiency (96%) and potential applications in other fields such as photoelectrochemistry, electrocatalysis, and optoelectronic devices.

Keywords: Pipe-like C_3N_4, Morphology tuning, Organic pollutants, Photocatalytic performance, Photocatalysis

1 Introduction

Semiconductor photocatalysis is a potential approach to address the environmental and energy challenges facing the world. The development of semiconductor photocatalytic materials as a green technology, cost-effective and simple approach for wastewater treatment and environmental remediation has advanced progressively[1,2]. Graphitic carbon nitride (g-C_3N_4) is an inexpensive, metal-free, earth-abundant and visible light harvesting photocatalyst that has received enormous attention over the last decade[3,4]. g-C_3N_4 possess characteristics such as small bandgap (~2.70 eV), excellent chemical and thermal stability. Nevertheless, the photocatalytic effectiveness of the pristine g-C_3N_4 for wider practical applicability is extremely low because of the high recombination rate of photogenerated electron–hole pairs, low surface area and electrical conductivity, less active sites and the inability for absorption above 460 nm[1,3,5,6].

Several techniques have been developed and tested to overcome the aforementioned drawbacks of pure g-C_3N_4. They include heterojunction establishment, doping and copolymerization, nanostructure construction and morphology control or tuning[5,7]. Until now, much effort has been put in to control the morphology of pure g-C_3N_4 resulting in the fabrication of several nanostructured designs such as nanotubes, nanowires, nanorods, nanosheets, nanospheres, etc.[1,6,8,9] with enhanced photocatalytic performance compared to the pristine g-C_3N_4.

In nature, there are various morphologies of materials. They include honeycomb, flower-like, core-shell, sheet-like, fiber and tube structures exist. These natural morphologies serve as prototypes for material designers and researchers to mimic because of their excellent performance. Pipe-like systems in nature contain channels that allow the flow of materials for effective performance. Thus, mimicking such a system in material design and fabrication can have enormous advantages and improved performance. In this study, pipe-like g-C_3N_4 was fabricated by the chemical method with enhanced properties for photocatalytic degradation of methylene blue (MB) as a source of wastewater.

2 Experimental

2.1 Fabrication of pipe-like g-C_3N_4

1 g of Dicyandiamide (DCDA) was dissolved in 20 ml of ethylene glycol to make a saturated solution by mixing for 5 min. Then 50 ml of 0.1M HNO_3 was then added to the prepared solution. After stirring for 10 min, the mixture was centrifuged and dried at 80 $^{\circ}$C for 16 h. The white powder obtained, which was then calcinated at 550 $^{\circ}$C for 2 h at a heating rate of 10 $^{\circ}$C min^{-1}. For comparison, a bulk g-C_3N_4 was also prepared at 550 $^{\circ}$C.

*Corresponding author (E-mail: makple@htu.edu.gh)

2.2 Characterization

Powder X-ray diffraction (XRD) was conducted on an X-ray diffractometer (Rigaku, Japan) using Cu Kα irradiation (λ = 0.15418 nm) at a scan rate of 0.05 s^{-1}. The element distribution map measurement was performed on a S4800 field emission scanning electron microscope (FESEM, Hitachi, Japan) equipped with an X-Max 50 energy-dispersive X-ray spectroscopy (EDS, Oxford Instruments, Britain) with an accelerating voltage of 10 kV. The Brunauer Emmett—Teller (BET) specific surface area (S_{BET}) of the samples were determined by nitrogen adsorption data in a *Micromeritics* ASAP 2020 nitrogen adsorption apparatus (USA). All the samples were degassed at 180 ^{o}C prior to the nitrogen adsorption measurements. The S_{BET} was investigated by a multipoint BET method using the adsorption data in the relative pressure (P/P_0) range of 0.05-0.3. A desorption isotherm was used to obtain the pore size distribution via the Barret—Joyner—Halender (BJH) method, assuming a cylindrical pore modal. The nitrogen adsorption volume at the relative pressure (P/P_0) of 0.99 was used to determine the pore volume and average pore size. X-ray photoelectron spectroscopy (XPS) measurements were done by using an ultra-high vacuum VG ESCALAB 210 electron spectrometer equipped with a multichannel detector, using Mg Kα (1253.6 eV) radiation (operated at 200 W) of a twin anode in the constant analyzer energy mode with a pass energy of 30 eV. All the binding energies were referenced to the C 1s peak at 284.8 eV of the surface adventitious carbon. The optical absorption property of the samples was obtained by a UV-visible absorption spectrophotometer (UV-2600, shimadzu, Japan). $BaSO_4$ was used as a reflectance standard in the UV-visible reflectance experiment. Fourier transform infrared spectra (FT-IR) of the samples were evaluated using an IR Affiinity-1 FT-IR spectrometer that used conventional KBr pellets in the range of 4000–500 cm^{-1} at room temperature. Photoluminescence (PL) emission spectra were used to investigate the fate of photogenerated electrons and holes in the samples. It was measured at room temperature on an F-7000 Fluorescence Spectrophotometer (Hitachi, Japan). The excitation wavelength was 380 nm, the scanning speed was1200 nm min^{-1}, and the photomultiplier tube (PMT) voltage was 700 V. The width of both the excitation slit and the emission slit was 1.0 nm.

2.3 Visible Light Degradation of Methylene Blue (MB)

Photocatalytic activity of the as-prepared samples under visible light was examined by measuring the rate of methylene blue (MB) degradation. 0.1 g of the as-prepared samples were dispersed into 100 mL aqueous solution of MB ($1x10^{-5}$ M). The suspension was stirred for 1 h in darkness to achieve adsorption equilibrium. The photoreaction process was carried out with continuous magnetic stirring under visible light (*i.e.* 300 W high pressure mercury lamp with a 420 nm cutoff filter which was placed 20 cm above the liquid surface. During the process, 3 mL of the solution was removed at a constant time (*i.e.* every 10 min for 50 min), where the photocatalyst was separated from the solution by centrifugation and the concentration of the remaining clear liquid measured by change in maximum absorbance at a wavelength of 663 nm by UV–Vis spectrometry (UV-3600, Shimadzu, Japan). The stability of the pipe-like g-C_3N_4 as-prepared sample was evaluated by conducting a reuse test of the samples for three cycles.

3 Results and Discussion

3.1 Phase and Microstructure Analyses

The crystal and phase structure of the pipe-like g-C_3N_4 was explored using XRD characterization as shown in Fig. 1. Two peaks located at 13.0^{o} and 27.5^{o} correspond to the (100) and (002) planes respectively in the bulk C_3N_4. The peaks are associated with the interplanar packing of heptazine (*i.e.* tri-s-heterocycle) units and π-π interlayer stacking motif for the (100) and (002) planes respectively in the bulk

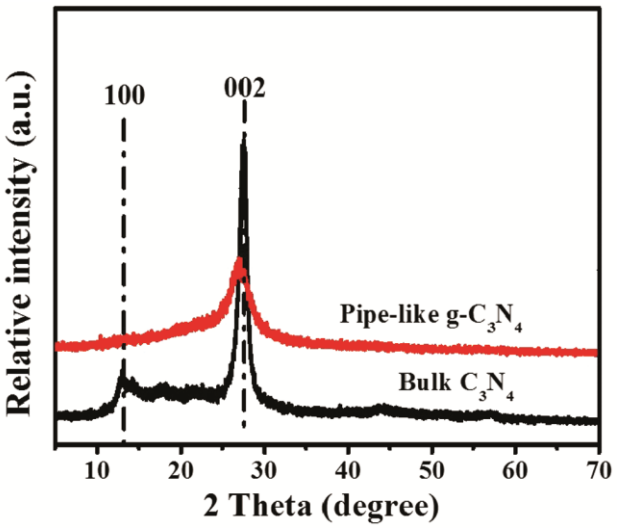

Fig. 1 — XRD patterns of pipe-like g-C_3N_4 and bulk C_3N_4.

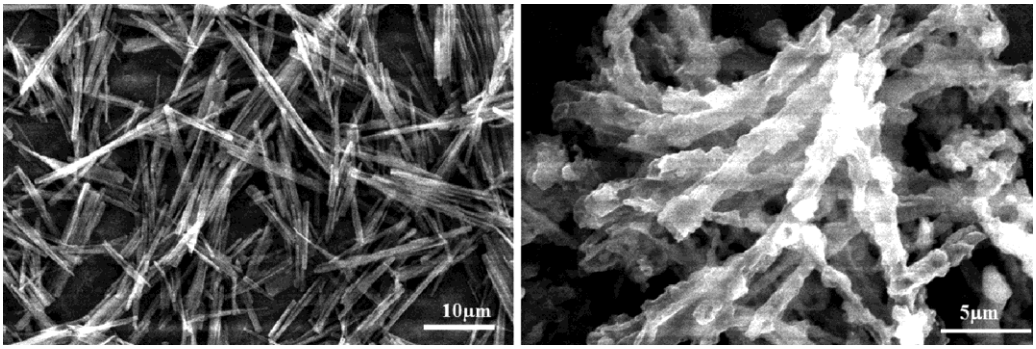

Fig. 2 — FESEM images of the pipe-like g-C_3N_4.

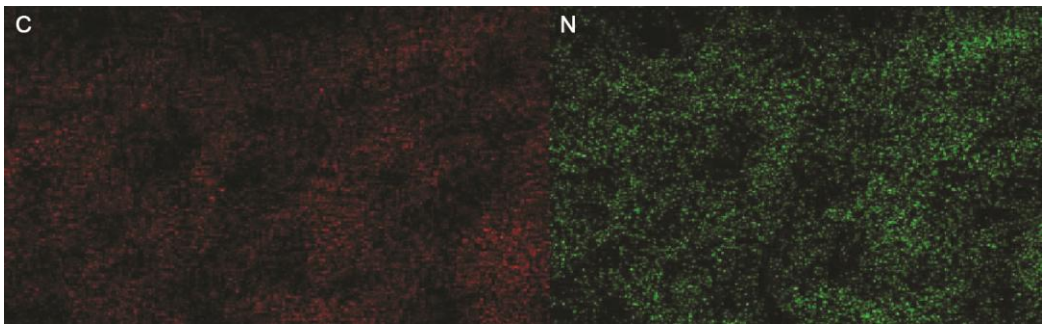

Fig. 3 — EDX elemental mapping images of the pipe-like g-C_3N_4.

C_3N_4[1,6]. In comparison with the pipe-like g-C_3N_4, the XRD pattern indicates only one broad and low intensity peak at 27.5° corresponding to the (002) plane. This is an indication for the reduction of the long interlayer stacking into short pipe-like structures.

The morphology and microstructure characterization was carried out by FESEM and shown in Fig. 2. It can be clearly observed from the FESEM images that the as-prepared sample g-C_3N_4 was pipe-like in nature with an average uniform length of 20 µm. The pipes can serve as channels for the flow of materials for enhanced photocatalytic performance.

It is obvious from the EDX elemental mapping images (Fig. 3) that there is a homogeneous distribution of both carbon (C) and nitrogen (N) as the only elements in the pipe-like g-C_3N_4. The C/N molar ratio from the elemental analysis for the pipe-like g-C_3N_4 is 0.70 with a stoichiometric C:N ratio being $C_{3.1}$:$N_{4.4}$. It can be observed from Fig. 4 that, the EDX composition graph for the pipe-like g-C_3N_4 shows only the presence of C and N which confirms the formation of the g-C_3N_4. The C/N molar ratio value determined was lower but close to the theoretical one of 0.75 for the pristine g-C_3N_4. The variance in the value is attributed to incomplete condensation that is normally associated with the preparation of g-C_3N_4[10,11].

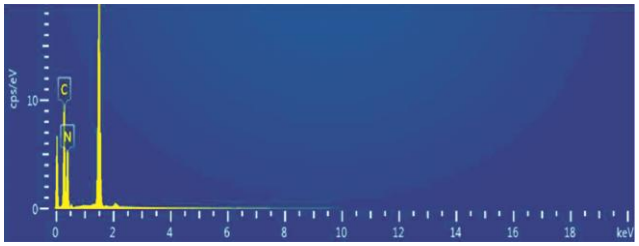

Fig. 4 — EDX composition graph for the pipe-like g-C_3N_4.

3.1.1 FT-IR and BET surface area analysis

To further reveal the microstructure of the samples prepared, the Fourier transform infrared (FT-IR) analysis was carried out. Figure 5 shows the FTIR spectra of pipe-like g-C_3N_4 and bulk C_3N_4. There are similarities in both spectra characteristics of the pipe-like g-C_3N_4 and bulk C_3N_4 indicating that both heptazine (or s-triazine) ring and trigonal C-N(-C)-C/bridging C-NH-C units were maintained in both samples. A sharp peak at 812 cm^{-1} characterized the heptazine or s-triazine ring. The several bands in 1213-1652 cm^{-1} are attributed to the stretching or bending vibration of the aromatic carbon and nitrogen heterocycles (*i.e.* C–N and/or C=N bonds)[1]. In addition, the broad band in a range of 3105-3700 cm^{-1} is attributed to the stretching vibrations of residual N–H bonds in the primary and secondary amines (=NH or $–NH_2$) groups and adsorbed water molecule[12]. The

FTIR analysis further confirmed that there is no obvious change in the microstructure of the pipe-like C_3N_4 and hence the maintenance of the basic atomic structure of g-C_3N_4.

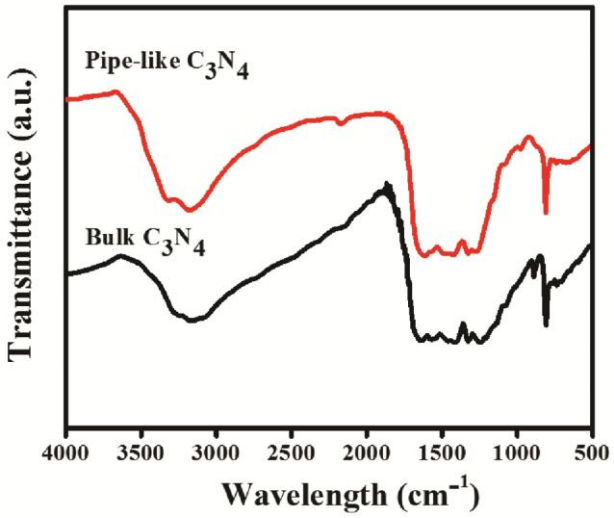

Fig. 5 — FTIR spectra of pipe-like g-C_3N_4 and bulk C_3N_4.

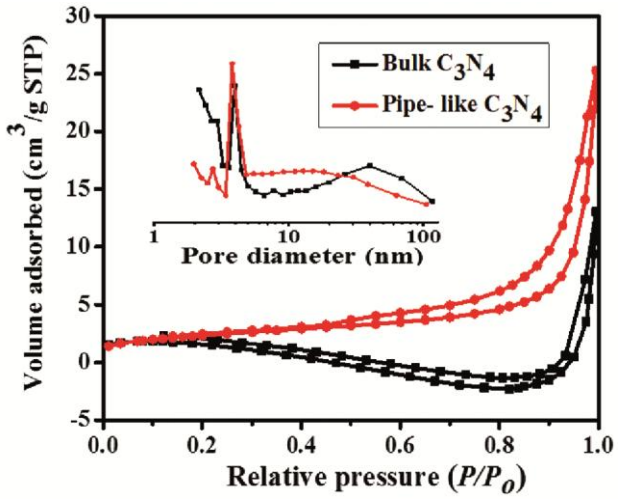

Fig. 6 — Nitrogen adsorption–desorption isotherms along with pore size distribution curves (inset) of pipe-like g-C_3N_4 and bulk C_3N_4.

It can be observed from Fig. 6 that the N_2 adsorption–desorption isotherms and the corresponding Barrett–Joyner–Halenda (BJH) pore size distribution curves show type IV isotherms according to Brunauer–Deming–Deming–Teller (BDDT) Classification. This suggests that mesopores are present within the samples prepared. The insert shown in Fig. 5 the pore size distribution curves of 3-10 nm also confirming the mesoporosity of the samples. The Brunauer−Emmett−Teller (BET) surface area of the pipe-like g-C_3N_4 is 8.4 m^2 g^{-1}, which is approximately twice the size area of the counterpart bulk C_3N_4 (ca. 4.7 m^2 g^{-1}) as well as the pore volume (Table 1). The large surface area of pipe-like C_3N_4 would lead to enhancement photocatalytic activity through surface absorption of reactants and exposure of more active sites and effective photocatalytic reaction.

3.1.2 XPS

The chemical state and composition of both bulk-C_3N_4 and Pipe-like C_3N_4 were characterized by XPS as shown in Fig. 7. Both the bulk-C_3N_4 and Pipe-like C_3N_4 show the same binding energy C 1s and N 1s peaks. This is an indication of a similar chemical state for carbon and nitrogen. The high resolution spectrum of C1s showed two peaks at 288.3 eV and 284.9 eV attributed to C–N–C coordination and surface adventitious carbon respectively for both samples[6,13]. Also, the fitted high resolution spectrum of the N1s

Table 1 — Physical properties of pipe-like C_3N_4 and bulk C_3N_4.

Samples	S_{BET} (m^2/g)	Pore volume (cm^3/g)	Pore size (nm)
Bulk C3N4	4.7	0.005	4.7
Pipe-like C3N4	8.4	0.02	10.3

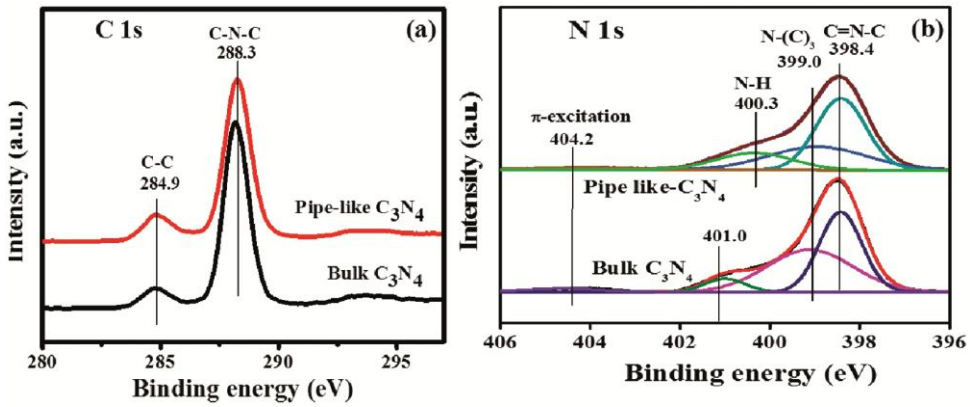

Fig. 7 — High resolution spectra of (a) C 1s and (b) N 1s for the Pipe-like C_3N_4 and bulk C_3N_4.

for both samples has three peaks a 398.4, 399.0 and at 400.3 eV attributed to C=N-C (sp^{2-} hybridized nitrogen), N-$(C)_3$ (tertiary nitrogen and N-H (amino functional groups) nitrogen respectively[13,6].

3.1.3 Optical property analysis

UV-Vis spectrophotometer was used to study the optical property of Pipe-like C_3N_4 and bulk C_3N_4 samples. From Fig. 8, it can be observed that the samples exhibited similarities in their absorption spectra. The absorption spectra extend from the UV region to the visible range up to 700 nm. A slight blue shift in the absorption edge from ca. 466 nm in the bulk C_3N_4 to 450 nm for the pipe-like C_3N_4 can be observed from the spectra. These results in a band gap energy increased from 2.66 eV to 2.75 eV for the bulk C_3N_4 and pipe-like C_3N_4 , respectively as shown in the Tauc plot (Fig. 9). The enhanced light-harvesting ability observed in the pipe-like C_3N_4 could be attributed to the thin layer of the pipes formed and the mesoporous nature. These properties would help improve upon the photocatalytic performance of the pipe-like C_3N_4.

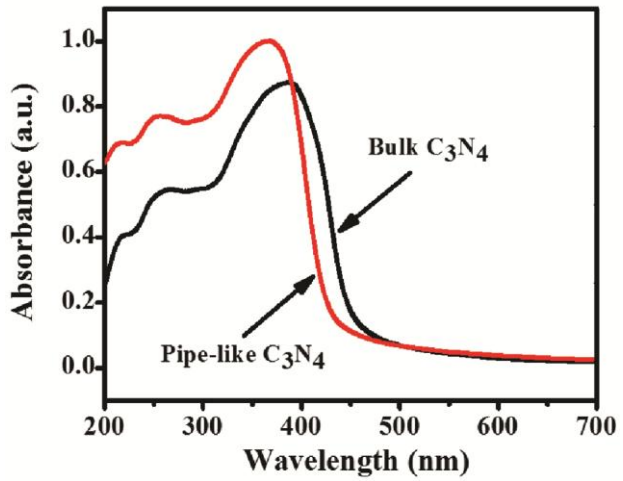

Fig. 8 — UV-Vis spectra of pipe-like g-C_3N_4 and bulk C_3N_4.

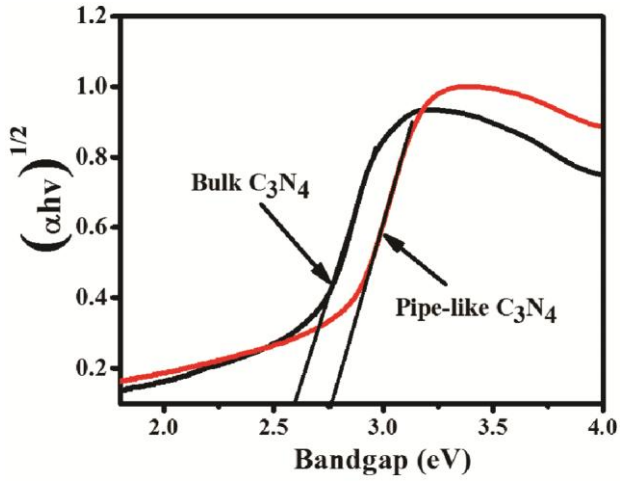

Fig. 9 — Tauc's plot showing the bandgap energy for the pipe-like g-C_3N_4 and bulk C_3N_4.

3.1.4 The photoluminescence (PL)

The PL measurement was carried out to determine the rate of recombination of photoexcited electron–hole pairs (*i.e.* charge carrier behaviours and separation efficiency) in the photocatalytic samples prepared. The stronger the PL peak intensity, the faster the recombination rate of photoexcited electron–hole pairs and therefore lower photocatalytic activity[14,15]. Figure 10 compared the PL spectra of pipe-like C_3N_4 and Bulk C_3N_4. A weak PL intensity emission peak was observed in the Pipe-like C_3N_4 sample relative to the bulk C_3N_4; an indication of decreased recombination of photogenerated electron-hole pairs (*i.e.* efficient separation of charge carriers) which would favour higher photocatalytic activity.

3.2 Evaluation of Photocatalytic Activity under Visible Light

The photocatalytic activity of the sample was evaluated by the photodegradation of methylene blue (MB) under visible-light irradiation. The changes in peak intensity of MB over the degradation time is illustrated in Fig 11 (a) for pipe-like C_3N_4 and (b) bulk C_3N_4. The Pipe-like C_3N_4 degraded MB within 30 min after exposure to the visible light, while bulk C_3N_4 utilized 50 min for complete degradation of MB.

The photodegradation kinetics of MB has followed the first order kinetic model as shown in Fig. 12. The

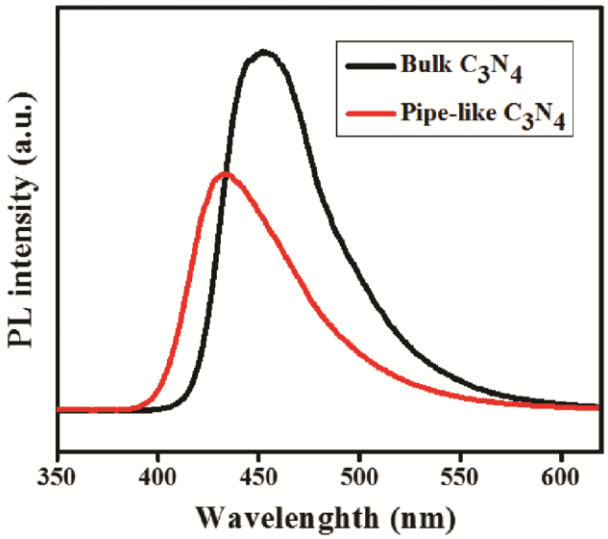

Fig. 10 — PL spectra of pipe-like g-C_3N_4 and bulk C_3N_4.

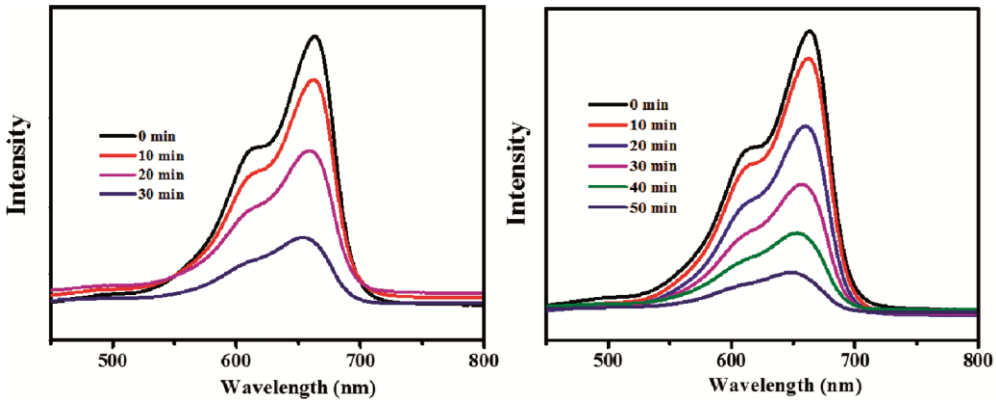

Fig. 11 — Photodegradation peak of MB using (a) Pipe-like C_3N_4 and (b) Bulk C_3N_4.

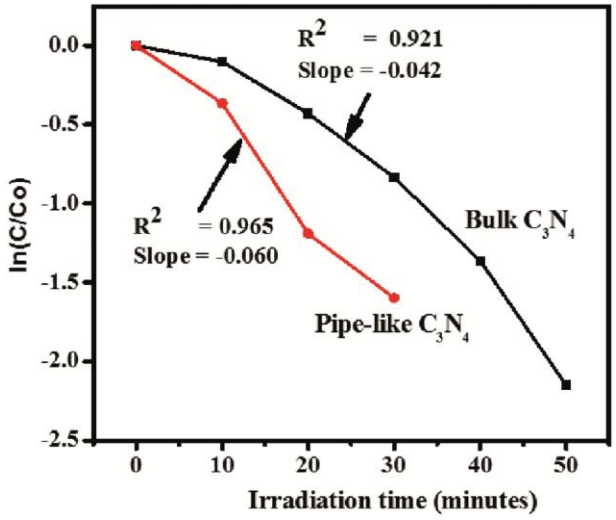

Fig. 12 — A Plot of $\ln(C_0/C)$ versus time for pipe-like C_3N_4 and bulk g-C_3N_4 for the degradation of MB.

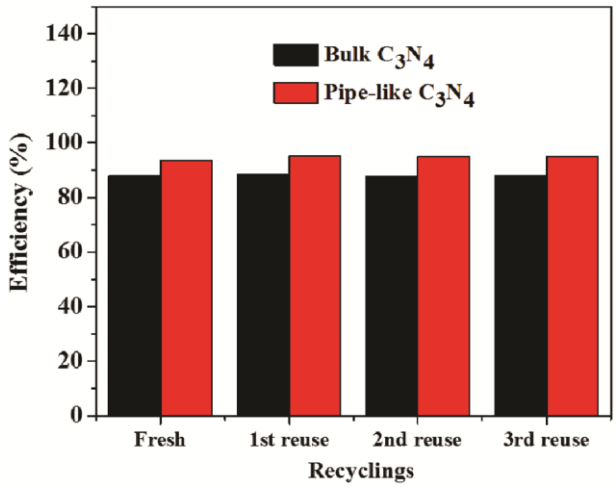

Fig. 13 — Results of the stability test for pipe-like C_3N_4 and bulk C_3N_4.

ln(C/Co) = kt, where C is the initial concentration of MB, and C_O is the concentration at any time, t. K is the rate constant and indicates the activity of the photocatalyst. A higher or lager negative slope (rate constant, K) indicates a faster rate of degradation. It can be observed that the Pipe-like C_3N_4 degraded the MB completely after 30 min, whereas the degradation for the bulk C_3N_4 was completed after 50 min. This clearly shows the superiority of the pipe-like C_3N_4 over the bulk C_3N_4 with a higher negative slope (K = -0.060 min^{-1}). The pipe-like C_3N_4 was recycled three (3) times for the degradation process as shown in Fig. 13. It was found that the pipe-like C_3N_4 was stable with 96% efficiency compared to the bulk C_3N_4. The recycling and stability test was carried out using the same amount of the samples, separated, washed and then used degrade the same concentration of the MB solution. The improved photocatalytic degradation process observed in the Pipe-like C_3N_4 is attributed to the large BET surface area that results in higher absorbability of the MB solution and large visible light harvesting property. In addition, tailored morphology also provides more active sites with efficient charge separation of electron-hole pairs.

4 Conclusions

A unique Pipe-like C_3N_4 was synthesized by a facile method that has high efficiency for visible light photocatalytic degradation of organic pollutants such as MB. The Pipe-like C_3N_4 degraded MB completely within 30 min with a 96% efficiency stability. This effective photocatalytic performance was achieved due to the morphology tuning of a graphitic carbon nitride into pipe-like nature that possesses exceptional properties such as high visible light-harvesting capacity, the large BET surface area which provides more active sites for species reaction and efficient charge separation of electron-hole pairs.

This novel Pipe-like C_3N_4 is envisaged to have a potential application in other fields such as photoelectrochemistry, electrocatalysis, and optoelectronic devices.

Acknowledgements

The author acknowledges contributions from members of the State Key Laboratory of Advanced Technology for Material Synthesis and Processing, Wuhan University of Technology, Wuhan 430070, PR China and Mechanical Engineering Department of Ho Technical University, Ghana for supporting the research in diverse ways.

Funding

The author would like to acknowledge financial support from the Ghana Government Book and Research Allowance for tertiary institutions.

References

1 Li Y Y, Zhou B X, Zhang H W, Ma S F, Huang W Q, Peng W, Hu W, & Huang G F, *Nanoscale*, 11 (2019) 6876
2 Samsudin M F R, Jayabalan P J, Ong W J, Ng Y H, & Sufian S, *J Photochem Photobiol A: Chem*, 378 (2019) 46
3 Zhang L, Jin Z, Huang S, Huang X, Xu B, Hu L, Cui H, Ruan S & Zeng Y J, *App. Catal B* 246 (2019) 61.
4 Akple M S, Low J, Wageh S, Al-Ghamdi A A, Yu J & Zhang J, *Appl Surf Sci*, 358 (2015) 196.
5 Jiang L, Yuan X, Pan Y, Liang J, Zeng G, Wu Z & Wang H, *Appl Catal B*, 217 (2017) 388.
6 Tahir M, Cao C, Butt F K, Idrees F, Mahmood N, Ali Z, Aslam I, Tanveer M, Rizwan M & Mahmood T, *J Mater Chem A*, 1 (2013) 13949.
7 Asadzadeh-Khaneghah S, Habibi-Yangjeh A & Seifzadeh D, *J Taiwan Inst Chem Eng*, 87 (2018) 98.
8 Kessler F K, Zheng Y, Schwarz D, Merschjann C, Schnick W, Wang X & Bojdys M J, *Nat Rev Mater*, 2 (2017) 17030.
9 Wang Y, Liu X, Liu J, Han B, Hu X, Yang F, Xu Z, Li Y, Jia S & Li Z, *Angew Chem*, 57 (2018) 5765.
10 Li X H, Wang X & Antonietti M, *Chem Sci*, 3 (2012) 2170.
11 Li X, Masters A F & Maschmeyer T, *Chem Cat Chem*, 7 (2015) 121.
12 Tu W, Xu Y, Wang J, Zhang B, Zhou T, Yin S, Wu S, Li C, Huang Y & Zhou Y, *ACS Sustain Chem Eng*, 5 (2017) 7260.
13 Zhao Y, Zhao F, Wang X, Xu C, Zhang Z, Shi G & Qu L, *Angew Chem*, 53 (2014) 13934.
14 Antil B, Kumar L, Reddy K, Gopinath C & Deka S, *ACS Sustain Chem Eng*, 7 (10) (2019) 9428.
15 Yu J, Wang K, Xiao W & Cheng B, *PCCP*, 16 (2014) 11492.